Supporting Information for

"How Do Pore Sizes Affect the Oxygen Reduction Reaction Kinetics of Platinum Electrodes?"

Kota Nakahara,[a,c] Atsunori Ikezawa,*[a,d] Junichi Inamoto,[b] Takeyoshi Okajima,[a] and Hajime Arai[a]

[a] School of Materials and Chemical Technology
Institute of Science Tokyo
Yokohama 226-8501, Japan
E-mail: ikezawa@mct.isct.ac.jp
[b] Graduate School of Engineering
University of Hyogo
Himeji 671-2280, Japan
[c] (Present address) Los Alamos National Laboratory
Los Alamos 87545, USA
[d] (Present address) Tokyo Metropolitan University
Hachioji 192-0397, Japan

Table S1. The surfactant used for fabricating the porous model electrode.

Electrode	Surfactant
Microporous 1.3 nm	$CH_3(CH_2)_{11}(OCH_2CH_2)_6OH$
Microporous 1.8 nm[1]	$CH_3(CH_2)_{11}(OCH_2CH_2)_8OH$
Mesoporous 3.0 nm	$CH_3(CH_2)_{15}(OCH_2CH_2)_8OH$ + n-heptane (1/1 mol)

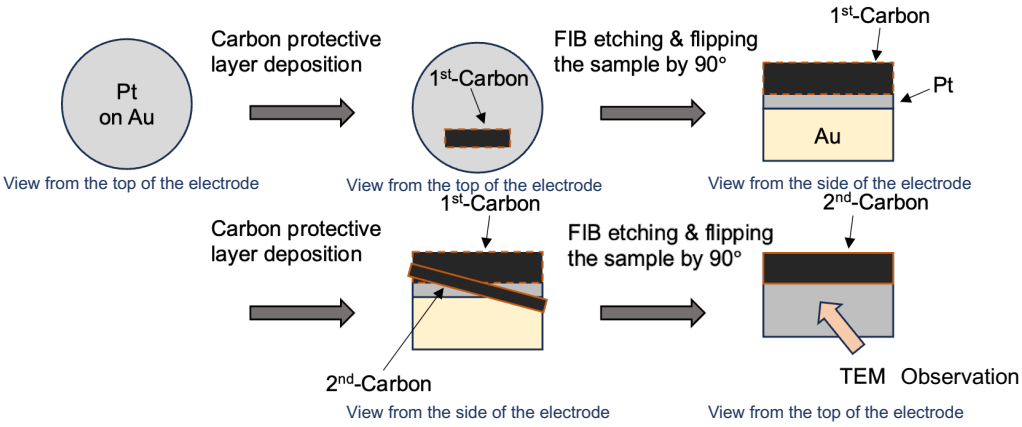

Figure S1. TEM sample preparation procedure using FIB. The sample was fabricated so that the TEM image can be obtained from the top of the electrode.

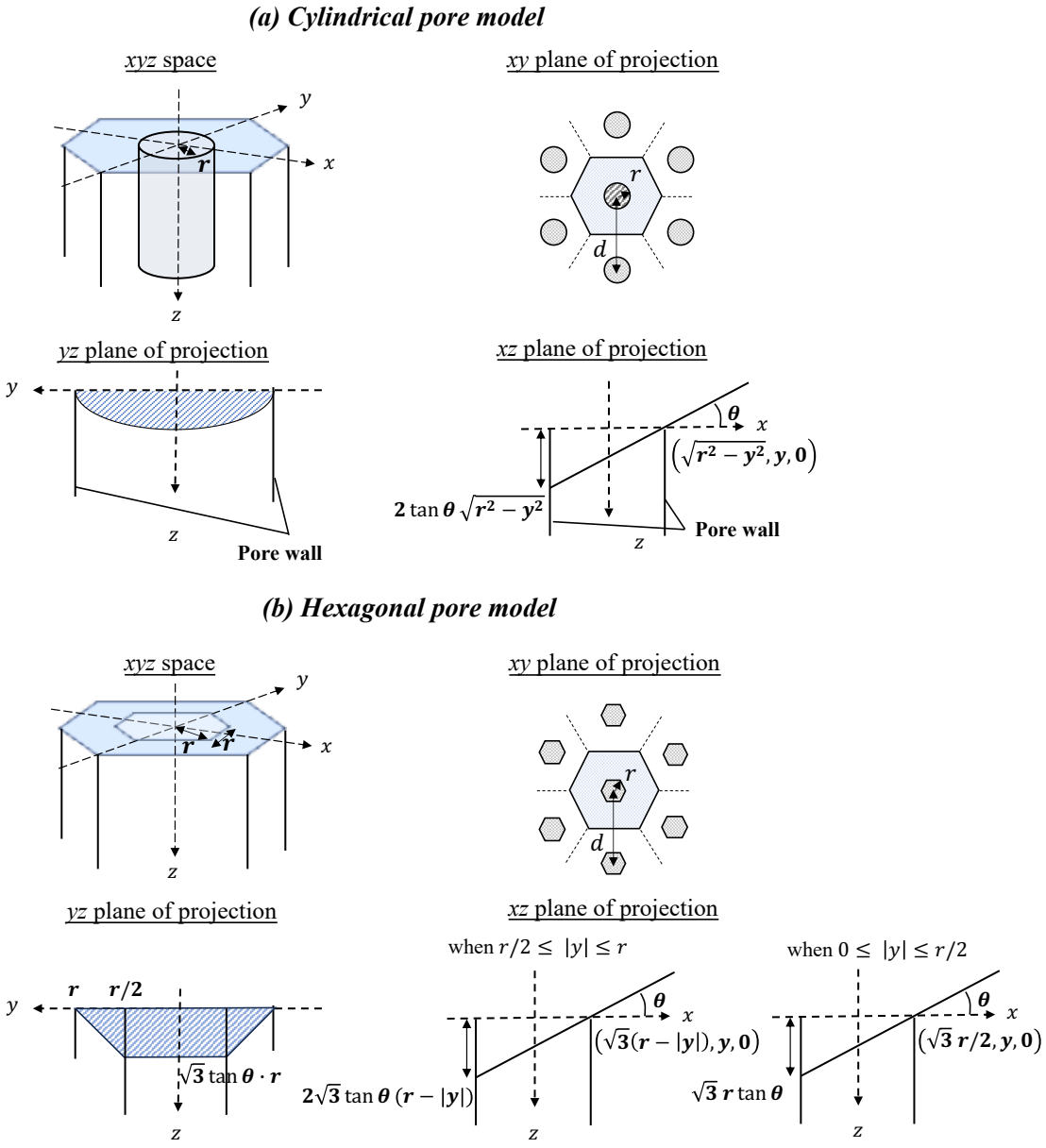

Figure S2. Unit cell of the (a) cylindrical and (b) hexagonal pore models, and their orientations in *xyz* coordinate and each plane of projection. On the *xz* and *yz* planes, the deepest pore end of the photoelectron emission and the pore wall on which the photoelectron emission occurs are depicted, respectively.

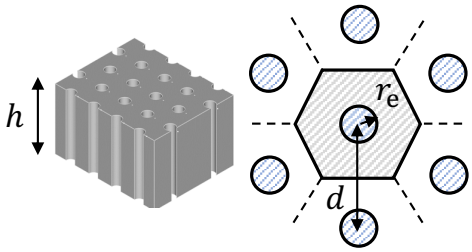

$$R_{f,geo} = \frac{2\pi r_e h + \left(\sqrt{3}d^2/_2 - \pi r_e^2\right)}{\sqrt{3}d^2/_2}$$

Figure S3. Unit cell of the model electrode and the calculation method of the roughness factor $R_{f,geo}$.

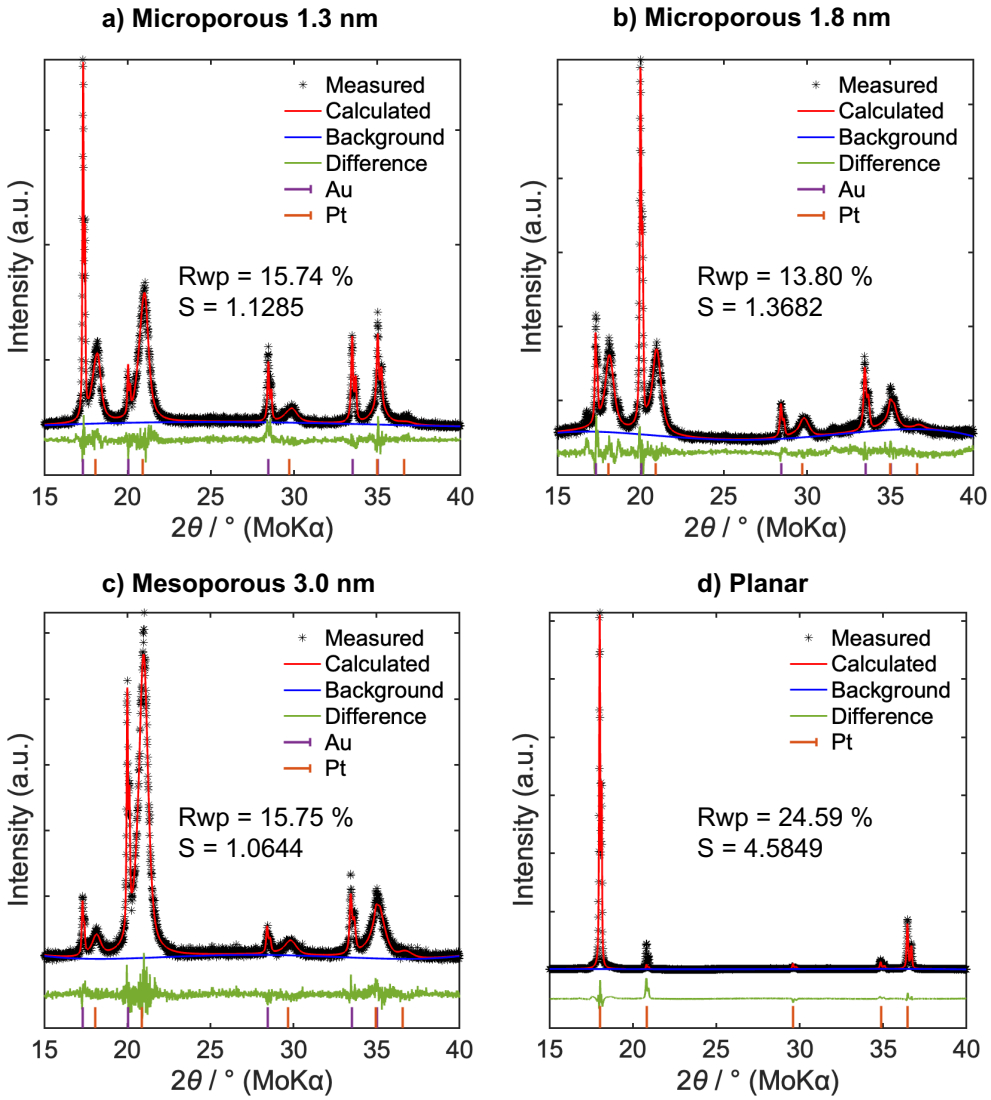

Figure S4. Rietveld refinement results of the model and planar electrodes. The model electrodes were obtained with a reduction charge density of 6.37 C cm^{-2} to increase the diffraction intensities.

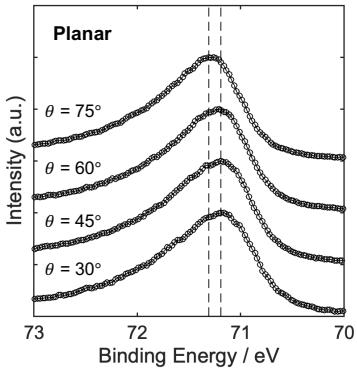

Figure S5. Angle-resolved X-ray photoelectron spectra of Pt $4f_{7/2}$ for the Pt planar electron. The data is sited from our previous study.[1]

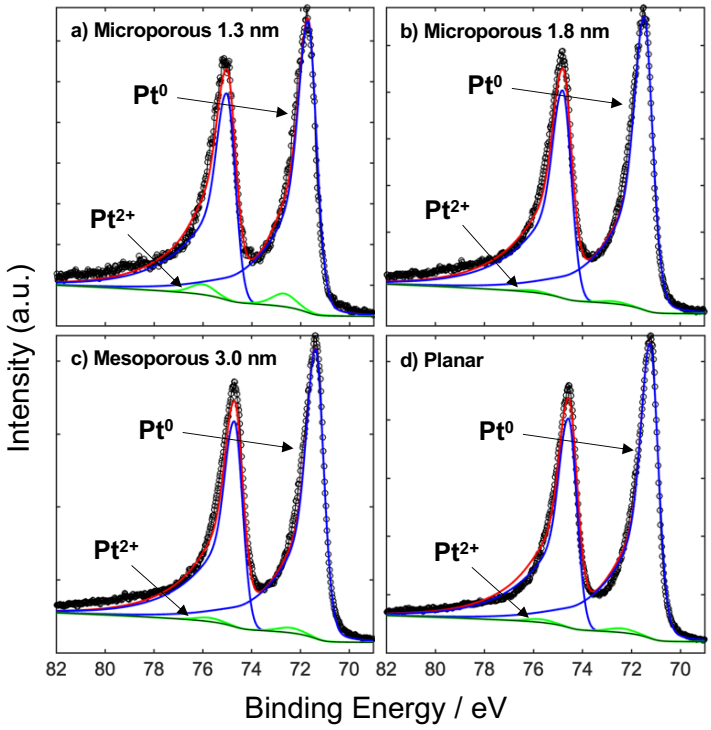

Figure S6. Deconvolution results of Pt 4f XPS spectra of a) microporous 1.3 nm (θ = 30°), b) microporous 1.8 nm (θ = 30°), c) microporous 3.0 nm (θ = 45°), and d) planer (θ = 45°). The data for the microporous 1.8 nm and planar electrode are cited from our previous study.[1]

Angle-resolved XPS calculation using the hexagonal pore model

The hexagonal pore model assumes that a pore forms a hexagon with the farthest diagonal distance defined as its pore size $2r$, where r represents its radius. As in the cylindrical pore model introduced in the Experimental section, an assumption is made that the photoelectrons can escape only from the outmost surface, and those blocked by the pore wall cannot each the detector. As shown in Figure S1, in a three-dimensional *xyz* space, the topmost surface of the unit cell is placed on the *xy* plane with the symmetrical centre at the origin. Herein, let the photoelectron emission plane make an angle θ with the *xz* plane. The deepest pore end, where the photoelectrons can be emitted to the detector at each *y*, is the cross-section between the pore wall and the emission line that goes through the rim of the pore,

$$z = \begin{cases} \sqrt{3}r\tan\theta & (\text{when } |y| \le r/2) \\ 2\sqrt{3}\tan\theta\,(r - |y|) & (\text{when } r/2 \le |y| \le r) \end{cases} \quad \text{(S)}$$

The area of the pore wall A_{wall} is calculated as follows,

$$A_{\text{wall}} = \sqrt{3}r\tan\theta \cdot r + 2 \cdot \frac{1}{2} \cdot \sqrt{3}r\tan\theta \cdot r = 2\sqrt{3}r^2\tan\theta \quad \text{(S)}$$

The observed binding energy is calculated as the average of the binding energy weighted with the measured area, using equation (S2), (3), (4) and (5).

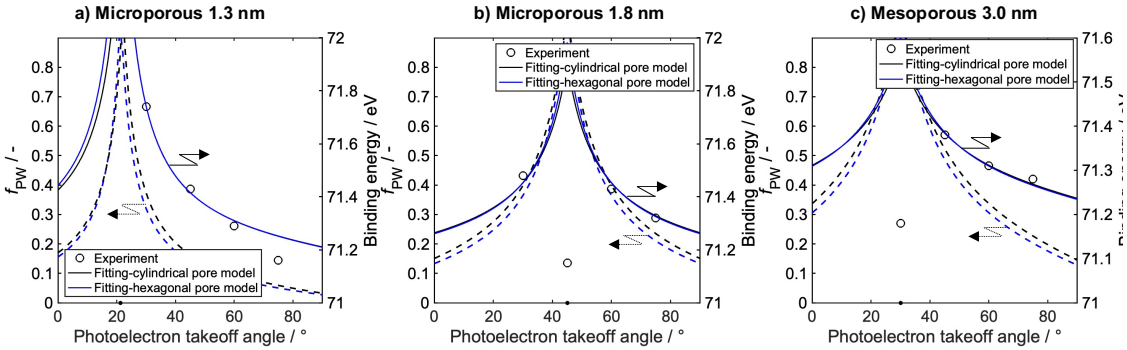

Figure S7. Comparison of the fitting to the angle-resolved XPS results between the cylindrical and hexagonal pore models for (a) microporous 1.3 nm, (b) microporous 1.8 nm, and (c) mesoporous 3.0 nm.

Table S2. Fitting parameters for the angle-resolved XPS results using the cylindrical and hexagonal pore models.

	Cylindrical pore model		Hexagonal pore model	
	BE_{wall} / eV	θ_{in} / °	BE_{wall} / eV	θ_{in} / °
Micro-porous 1.3 nm	72.7	68.0	73.0	68.7
Micro-porous 1.8 nm	71.9	45.0	72.0	45.0
Meso-porous 3.0 nm	71.6	60.0	71.6	60.0

Numerical simulation of the oxygen concentration gradient

ORR currents and oxygen concentration profiles were calculated under the steady state condition using finite-difference methods, as conducted in our previous study.[1] The symbols and values used are shown in Table S2. The calculation model is constructed by translating the hexagonal unit cell of the model electrode into a cylindrical cell (Figure S6). In the approximation, the length of the *r*-axis R is determined by assuming that both cells have the same base area,

$$\pi R^2 = \frac{\sqrt{3}}{2} d^2 \;\leftrightarrow\; R \approx 0.525\, d \tag{S1}$$

The reaction is assumed to proceed under the steady state condition. The length of the *z*-axis outside of the pore is then determined as the diffusion layer thickness δ for rotating disk electrode systems,[2]

$$\delta = 1.61 D^{1/3} \nu^{1/6} \omega^{-1/2} \tag{S2}$$

The reaction rates of ORR at the pore wall and the outer surface of the electrode are described by the Tafel equation, which are equal to the diffusion current under the steady state condition,

at $r = r_\mathrm{e}$ and $0 \le z \le h$

$$nFD \frac{\partial c}{\partial r} = -i_0 \frac{c}{C^\mathrm{b}} \exp\left(-\frac{\alpha n F \eta}{RT}\right) \tag{S3}$$

at $z = h$ and $r_\mathrm{e} \le r \le R$

$$-nFD \frac{\partial c}{\partial z} = -i_0 \frac{c}{C^\mathrm{b}} \exp\left(-\frac{\alpha n F \eta}{RT}\right) \tag{S4}$$

In the above description, the local oxygen concentration is different and needs to be solved. In addition, the electrolyte resistance in the pore is less significant than that of the bulk electrolyte. For that reason, the effective overpotential at each section is assumed to be invariable.

The oxygen transport in the pore is described by the Fick's second law in its appropriate form for the cylindrical coordinate system,

$$\frac{\partial c}{\partial t} = D\left(\frac{\partial^2 c}{\partial r^2} + \frac{1}{r}\frac{\partial c}{\partial r} + \frac{\partial^2 c}{\partial z^2}\right) = 0 \tag{S5}$$

The bottom of the pore is comprised of gold, and its ORR activity can be negligible compared to that of platinum. In that case, the flux of oxygen is invariable across the surface,

at $z = 0$

$$\frac{\partial c}{\partial z} = 0 \tag{S6}$$

The oxygen diffusion appears to not occur across the center and outer axis due to the symmetrical cylindrical coordinate system,

at $r = 0, R$

$$\frac{\partial c}{\partial r} = 0 \tag{S7}$$

The concentration beyond the diffusion layer is equal to the bulk concentration,

at $z = h + \delta$

$$c = C^\mathrm{b} \tag{S8}$$

The concentration profile and the corresponding current were obtained at each potential. The current was calculated by integrating the partial current and dividing it by the geometric surface area (Figure S7).

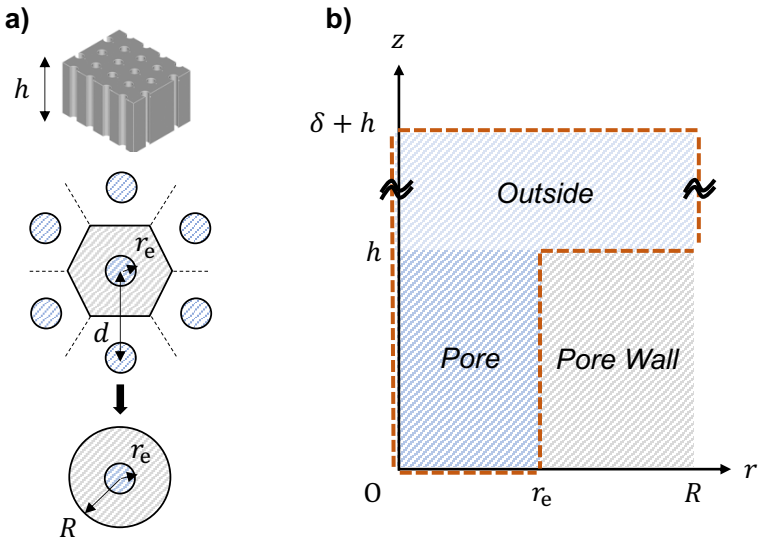

Figure S8. Conceptual image of a cylindrical approximation of the hexagonal unit cell of the model electrode.

(b) Numerical simulation model in the cylindrical coordinate system.[1]

Table S3. List of symbols and values used in the numerical simulation.

Symbol	Description	Value
r_e	Pore radius	0.65 nm
h	Electrode thickness / Pore length	40 nm
d	Pore distance	5.0 nm
R	Model radius	2.625 nm
D	Diffusion coefficient	1.83×10^{-5} cm^2 s^{-1} (0.1 M KOH)[3] 1.93×10^{-5} cm^2 s^{-1} (0.1 M $HClO_4$)[4]
υ	Kinematic viscosity	0.0090 cm^2 s^{-1} (0.1 M KOH)[5] 0.010 cm^2 s^{-1} (0.1 M $HClO_4$)[4]
ω	Rotation speed	209.4 rad s^{-1} (2000 rpm)
δ	Diffusion layer thickness	13.4 μm (0.1 M KOH) 13.9 μm (0.1 M $HClO_4$)
c	Oxygen concentration	–
C^b	Oxygen concentration in the bulk solution	1.21 mol m^{-3} (0.1 M KOH)[3] 1.10 mol m^{-3} (0.1 M $HClO_4$)[4]
n	Electron transfer number	4
F	Faraday constant	96485 C mol^{-1}
η	Overpotential	–
$\frac{2.303\ RT}{\alpha nF}$	Tafel slope	56.08 mV dec^{-1} (0.1 M KOH) 60.35 mV dec^{-1} (0.1 M $HClO_4$)
i_0	Exchange current density	1.349×10^{-6} mA cm^{-2} (0.1 M KOH) 3.246×10^{-6} mA cm^{-2} (0.1 M $HClO_4$)

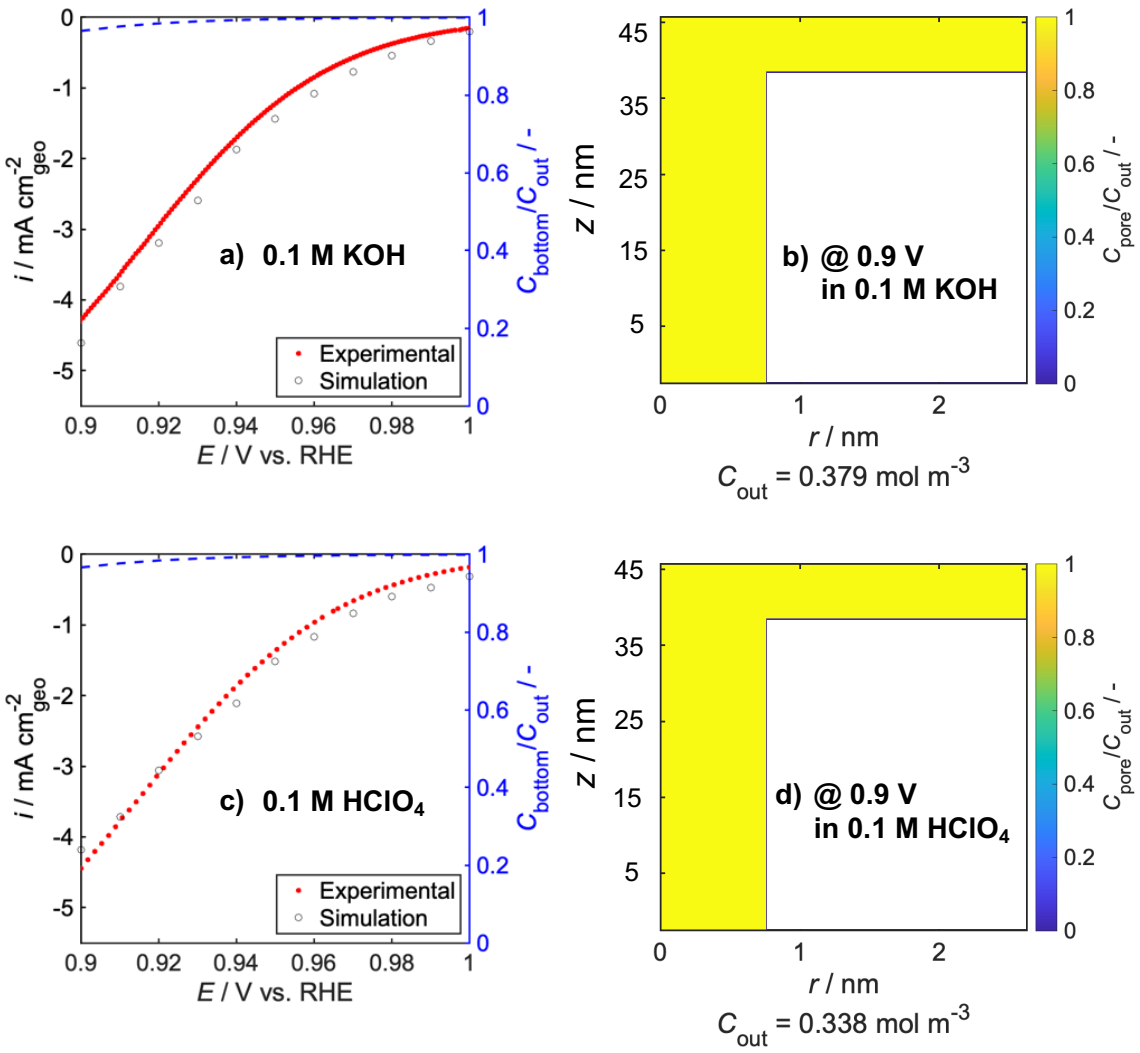

Figure S9. Calculated current densities and oxygen concentration profiles at 0.90 V in (a,b) 0.1 M KOH and (c,d) 0.1 M $HClO_4$ solutions for microporous 1.3 nm.

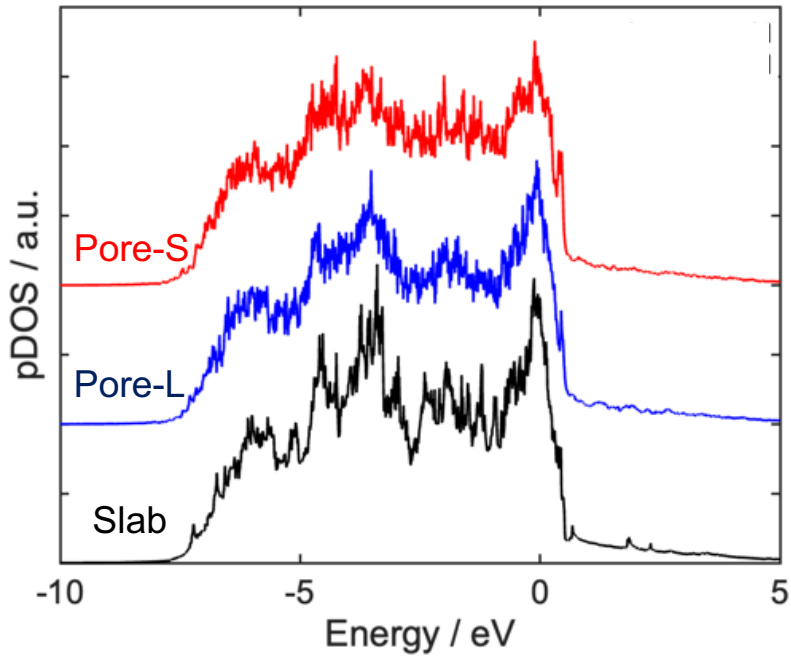

Figure S10. Calculated partial density of state (pDOS) of the d-band of the porous and slab models.

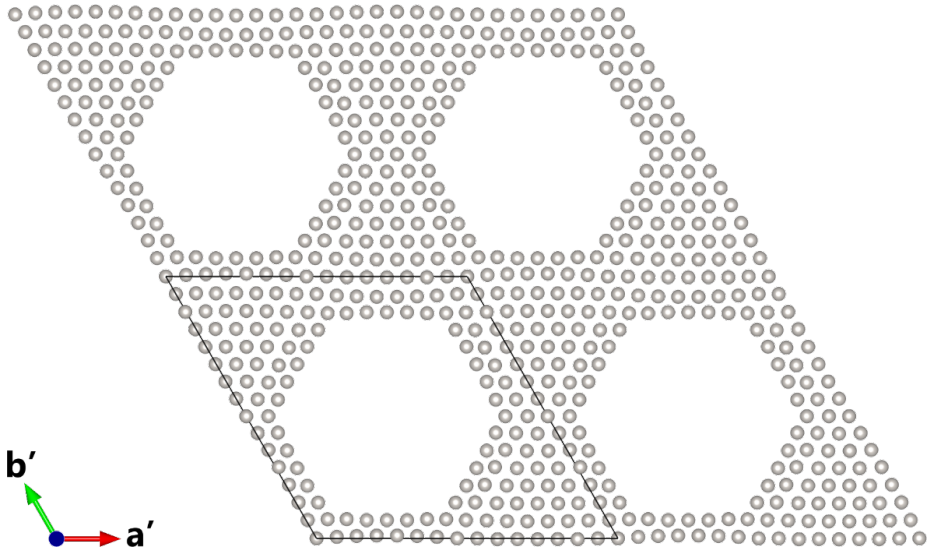

Figure S11. Relaxed structures of the Pore-M.

Table S4. Structural parameters of the Pore-M. Here, “lattice constant a from *a*' and *b*', or *c*'” are values corresponding to the lattice constant *a* of FCC Pt, which is calculated from the lattice constants *a*' and *b*' or *c*' by axial transformation.

Model	Pore size / nm	Pore distance / nm	Inter-pore thickness / nm	Lattice constant *a* from *a*' and *b*' / nm	Lattice constant *a* from *c*' / nm
Pore-M	1.86	2.36	0.504	0.386	0.384

References

1. K. Nakahara, A. Ikezawa, T. Okajima and H. Arai, *ChemElectroChem*, 2024, **11**, e202300654.
2. A. J. Bard and L. R. Faulkner, “Electrochemical methods: fundamentals and applications”, Wiley, New York, 2nd edn., 2001.
3. R. E. Davis, G. L. Horvath and C. W. Tobias, *Electrochim. Acta*, 1967, **12**, 287-297.
4. M. R. Rahman, M. I. Awada, F. Kitamura, T. Okajima and T. Ohsaka, *J. Power Sources*, 2012, **220**, 65-73.
5. D. Zhang, J. F. Wu, L. Q. Mao, T. Okajima, F. Kitamura, T. Ohsaka and T. Sotomura, *Indian J. Chem. Sec A.*, 2003, **42A**, 801-806.